J|A|C|S ARTICLES

Published on Web 08/05/2009

Experimental Thermodynamics of High Temperature Transformations in Single-Walled Carbon Nanotube Bundles

Daniele Gozzi,*,† Alessandro Latini,† and Laura Lazzarini‡

Dipartimento di Chimica, SAPIENZA Università di Roma, Piazzale Aldo Moro 5, 00185 Roma, Italy, and IMEM-CNR, Parco Area delle Scienze 37/A, Localita' Fontanini, 43010 Parma, Italy

Received May 27, 2009; E-mail: daniele.gozzi@uniroma1.it

Abstract: The thermodynamic quantities associated to the transformation of carbon in single-walled carbon nanotube (SWCNT) bundles to carbon in graphite were determined from 750 to 1015 K by a CaF_2 solid electrolyte galvanic cell: (−) Mo | Cr_3C_2,CrF_2,C″ | CaF_2s.c. | Cr_3C_2,CrF_2,C′ | Mo (+). The trend with temperature of the electromotive force of the cell was found to be greatly dependent on temperature and fully reversible with it. The standard enthalpy ΔH°_T and entropy ΔS°_T changes are 7.1, 6.0, and 60.2 kJ mol^{-1} and 8.6, 14.7, and 72.8 J K^{-1} mol^{-1} at 778, 883, and 975 K, respectively. This most likely correlates with the different arrangements and shapes of tubes that deviate from the ideal triangular closed packed structure of the SWCNT bundles. The constraints to the thermal expansion of bundles in the electrode containing them generated high internal pressures that were responsible for deformations of tube shape and lattice. Stable bundle states were formed that interconvert as a function of temperature. Comparative analyses by low angle XRD, microRaman, and HR-TEM of SWCNT bundles before and after experiments support this scenario. The cohesion energy and associated entropy changes are also reported for such states. The formation enthalpy of unbundled SWCNTs was calculated equal to 9.5 ± 0.4 kJ mol^{-1}.

1. Introduction

Since the discovery of the carbon nanotubes (CNTs) in 1991 by Iijima,[1] the scientific community has displayed a growing interest in this allotropic form of carbon through many publications covering basic[2,3] and theoretical[4,5] aspects as well as applications.[6,7] It is usual to distinguish CNTs in single-walled (SWCNTs) and multiwalled (MWCNTs) depending on how many graphene planes are coaxially assembled.

Graphite represents the reference state of any type of CNT, graphite being the stable form of carbon resulting from the assembly of graphene planes piled up along the orthogonal *c*-axis. A weak interlayer energy, W_L, ranging from 4.10^8 to 21.0^9 kJ mol^{-1}, holds together the graphene planes whereas a strong C−C bond energy, W_B, links carbon atoms in the planes. Any deviation from planarity increases the energy of the assembly of the graphene layers, which is due to the distance between layers and to the bending of sp^2 planar bond structure. CNTs are generated by such a large deviation from the planarity of the assembly of graphene planes such as to form a cylindrical shape. Therefore, it is expected that CNT energy content is higher than that of graphite.

Some theoretical approaches[10,11] are reported in the literature to calculate the CNT energy as function of diameter and length and as a function of the number of walls in the case of MWCNTs. Recently,[12] we reported the thermodynamic quantities, such as the changes of standard free energy, $\Delta_r G^\circ$, standard enthalpy, $\Delta_r H^\circ$, and standard entropy, $\Delta_r S^\circ$ that were experimentally obtained for the transformation from graphite to MWCNTs in the temperature range 820−920 K by making use of solid electrolyte galvanic cells (SEGCs). The availability of high purity MWCNTs produced[13] in a reasonable quantity and tested[14] to be practically without amorphous and/or graphitic carbon made possible such determinations. The absence of amorphous carbon and a satisfactory uniformity in sizes and number of walls are explained by the peculiar nucleation and growth mechanism[15] due to both the catalyst and low temperature (∼500 °C) at which MWCNTs grow.

The scope of the present work is to study the thermodynamics of SWCNT bundles with respect to graphite. Differently from MWCNTs, SWCNTs usually self-assemble into a two-dimensional hexagonal close-packed lattice forming bundles with intertube spacing 0.32 nm, typical of van der Waals interac-

† SAPIENZA Università di Roma.
‡ IMEM-CNR.

(1) Iijima, S. *Nature* **1991**, *354*, 56.
(2) Belin, T.; Epron, F. *Mater. Sci. Eng., B* **2005**, *119*, 105.
(3) Harris, J. F. *Carbon* **2007**, *45*, 229.
(4) Sun, C. H.; Finnerty, J. J.; Lu, G. Q.; Cheng, H. M. *J. Phys. Chem. B* **2005**, *109*, 12406.
(5) Reich, S.; Li, L.; Robertson, J. *Phys. Rev. B* **2005**, *72*, 165423.
(6) Tasis, D.; Tagmatarchis, N.; Bianco, A.; Prato, M. *Chem. Rev.* **2006**, *106*, 1105.
(7) Raffaelle, R. P.; Laudi, B. J.; Harris, J. D.; Bailey, S. G.; Hepp, A. F. *Mater. Sci. Eng., B* **2005**, *116*, 233.
(8) Girifalco, L. A. Ph.D. thesis, University of Cincinnati, 1954.
(9) Setton, R. *Bull. Soc. Chim. Fr.* **1960**, *1758*, 521.
(10) Setton, R. *Carbon* **1996**, *34*, 69.
(11) Zhang, S.; Zhao, S.; Xia, M.; Zhang, E.; Xu, T. *Phys.Rev. B* **2003**, *68*, 245419.
(12) Gozzi, D.; Iervolino, M.; Latini, A. *J. Am. Chem. Soc.* **2007**, *129*, 10269.
(13) Gozzi, D.; Latini, A. PCT Int. Appl. (2006), WO 2006040788 A1 20060420.
(14) Gozzi, D.; Latini, A.; Lazzarini, L. *Chem. Mater.* **2008**, *20*, 4126.
(15) Tomellini, M.; Gozzi, D.; Latini, A. *J. Phys. Chem. C* **2007**, *111*, 3266.

10.1021/ja904294z CCC: $40.75

Table 1. Product Data Sheet of SWCNT Sample

outside diameter, nm	1−2
length, μm	5−30
SWCNT content, wt%	>90
ash, wt%	<1.5
elemental analysis, %	C (96.31), Al (0.10), Cl (0.40), Co (2.90), S (0.29)
specific surface area, $m^2\ g^{-1}$	>407
electrical conductivity, $ohm^{-1}\ cm^{-1}$	$>10^2$

tions.[16] In most studies, cylindrical tubes with a circular cross-section are assumed because this is the shape that minimizes the strain energy of free, isolated tubes. There are several experimental[17−20] and theoretical[21−24] investigations where tubes in a bundle may deform from the ideal circular cross section to a polygonized, hexagonal cross section. This raises the question of what is the equilibrium configuration of a lattice of aligned tubes and the possibility of the existence of several metastable structures depending on the experimental conditions.[24]

For the past several years, the electromotive force (E) technique using SEGCs has been routinely practiced in our laboratory;[25,26] more recently the technique has also been successfully utilized in the CNT field[12,27] as well as in the present study to determine the thermodynamics of SWCNT bundles at high temperatures.

2. Experimental Section

SWCNTs were purchased from Cheap Tube (Brattleboro, VT), and their product data sheet is reported in Table 1. The as-received sample was carefully characterized before use by thermogravimetry (TG-DTG), high resolution transmission electron microcopy (HR-TEM), X-ray diffraction (XRD), and microRaman (mR). TG and DTG only will be reported in this section.

Thermogravimetric measurements were performed by a Netzsch STA 409 PC Luxx thermobalance (temperature range: RT to 1500 °C; resolution: 2 μg) in simultaneous DTA-TG mode. Temperature was measured by means of a S-type thermocouple (Pt−Pt/Rh 10%). The thermocouple was calibrated against the melting points of In, Sn, Bi, Zn, Al, Ag, Au, and Ni. All the measurements were performed in alumina crucibles. The CO_2 flow rate used in the experiments was 42 sccm. A correction measurement without sample was performed and subtracted to the TG and DTG curves of the samples.

TEM analyses were performed by a JEOL JEM 2200FS field emission transmission electron microscope operating at 200 kV (resolution: 0.19 nm). Samples for imaging were prepared by ultrasonic dispersion of small amounts of powders in 2-propanol and then putting a drop of the dispersion on holey carbon-coated copper grids.

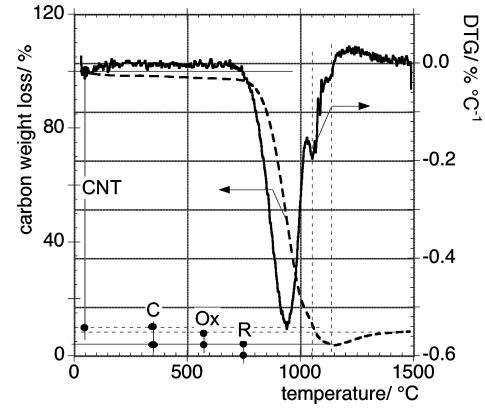

Figure 1. Thermogravimetric analysis in pure CO_2 of the as-received sample of SWCNT bundles, which were mixed with chromia to catalyze the Boudouard reaction.[14] Thermogravimetric data are reported on the left axis while their derivative (DTG) is on the right axis. The differentiation between CNT, carbon (C), residue (R), and fraction in the latter (Ox) that is oxidized by CO_2 is reported. The SWCNT carbon in the as-received sample was 90.0 wt % and total carbon was 96.0 wt %.

X-ray diffraction patterns were acquired using a Panalytical X'Pert Pro diffractometer (Bragg−Brentano geometry, radiation Cu Kα, $\lambda = 0.154184$ nm) equipped with two gas-filled proportional detectors. The first one, equipped with a programmable receiving slit, is suited for $\theta-\theta$ type scans; the second one, equipped with a graphite monochromator, is reserved to measurements with a fixed glancing incidence angle. Kβ radiation is cut by a Ni filter when using the first detector. The low angle spectra were acquired in glancing incidence angle mode (3°) using the second detector, an incident beam mask of 1/32°, and a 20 mm incident beam mask. The sample holder was made of amorphous Si (Panalytical) in order to avoid interference.

The samples were characterized by making use of a Renishaw inVia Raman Microscope (UK) equipped with Ar laser ($\lambda = 514.5$ nm, Ar^+, 2.41 eV).

The determination of SWCNT content in the as-received sample was performed according to the procedure reported in literature,[14] which is based on the Boudouard reaction catalyzed by chromia. Figure 1 shows TG (left axis) and DTG (right axis) measurements carried out in pure CO_2 on a mixture of SWCNTs and Cr_2O_3. The as-received SWCNT content in the mixture was 32.77 wt %. The figure clearly indicates that the differentiation between CNT, carbon (C), residue (R), and fraction in the latter (Ox) that is oxidized by CO_2 when carbon is no longer present, and the local CO/CO_2 ratio, becomes zero. The SWCNT carbon in the as-received sample was 90.0 wt % and total carbon was 96.0 wt %.

2.1. Galvanic Cells. The general scheme of a SEGC with CaF_2 single crystal (s.c.) as solid electrolyte suitable to determine the difference of the carbon chemical potential, $\Delta\mu_C$, is:[12]

$$(-)\mathrm{Mo}|\mathrm{Cr_3C_2},\mathrm{CrF_2},\mathrm{C''}|\mathrm{CaF_2\,s.c.}|\mathrm{Cr_3C_2},\mathrm{CrF_2},\mathrm{C'}|\mathrm{Mo}(+) \quad \text{(A)}$$

where C′ and C″ is carbon in two allotropic forms.

The electrode containing carbon as graphite was already studied[28] in cells for determining the thermodynamic properties of Cr_3C_2 in combination with reference electrode Cr−CrF_2. Cell A is a fluorine concentration cell where the positive electrode is the electrode where the chemical potential of F_2(g) is higher and that of carbon is lower. This implies that $\Delta\mu_C = -{}^3/_2\Delta\mu_{F_2}$. In the present work where

(16) Thess, A.; Lee, R.; Nikolaev, P.; Dai, H.; Petit, P.; Robert, J.; Xu, C.; Lee, Y. H.; Kim, S. G.; Rinzler, A. G.; Colbert, D. T.; Scuseria, G. E.; Tomanek, D.; Fischer, J. E.; Smalley, R. E. *Science* **1996**, *273*, 483.
(17) Chesnokov, S. A.; Nalimova, V. A.; Rinzler, A. G.; Smalley, R. E.; Fisher, J. R. *Phys. Rev. Lett.* **1999**, *82*, 343.
(18) Tang, J.; Qin, L. C.; Sasaki, T.; Yudasaka, M.; Matsushita, A.; Iijima, S. *Phys. Rev. Lett.* **2000**, *85*, 1887.
(19) Sharma, S. M.; Karmakar, S.; Sikka, S. K.; Teredesai, P. V.; Sood, A. K.; Govindaraj, A.; Rao, C. N. R. *Phys. Rev. B* **2001**, *63*, 205417.
(20) Rols, S.; Goncharenko, I. N.; Almairac, R.; Sauvajol, J. L.; Mirebeau, I. *Phys. Rev. B* **2001**, *64*, 153401.
(21) Tersoff, J.; Ruoff, R. S. *Phys. Rev. Lett.* **1994**, *73*, 676.
(22) Lu, J. P. *Phys. Rev. Lett.* **1997**, *79*, 1297.
(23) Girifalco, L. A.; Hodak, M.; Lee, R. S. *Phys. Rev. B* **2000**, *62*, 13104.
(24) Lòpez, M. J.; Rubio, A.; Alonso, J. A.; Qin, L.-C.; Iijima, S. *Phys. Rev. Lett.* **2001**, *86*, 3056.
(25) Di Pascasio, F.; Gozzi, D.; Parodi, N.; Borzone, G. *J. Phys. Chem. B* **2002**, *106*, 4284.
(26) Gozzi, D.; Iervolino, M. *Intermetallics* **2005**, *13*, 1172.
(27) Gozzi, D.; Latini, A.; Tomellini, M. *J. Phys. Chem. C* **2009**, *113*, 45.
(28) Kleykamp, H. *J. Alloys Compd.* **2001**, *321*, 138.

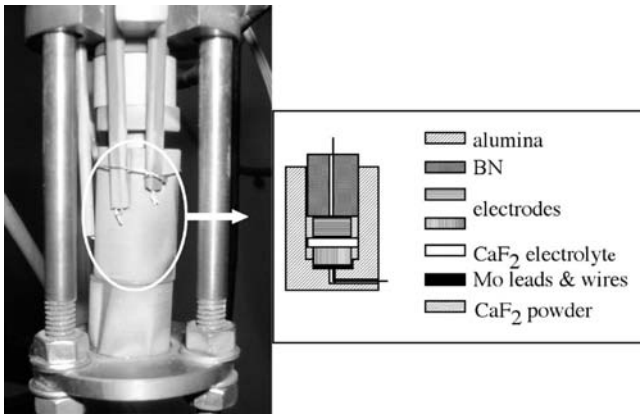

Figure 2. The galvanic cell assembly inside the latticework is shown. Three S-type thermocouples are positioned close to the cell. Two of them are used to check the isothermal condition of the cell. The third thermocouple is utilized to drive the furnace power control. A scheme of the cell holder is also reported with effusion hole on the top. This hole is also the way out for the Mo lead.

$C' \equiv C_{CNT}$ (carbon in the SWCNT bundles) and $C'' \equiv C_G$ (carbon in graphite), the cell reaction can be written as:

$$\begin{gathered} 3e + \frac{3}{2}CrF_2 + C_{CNT} = 3F^- + \frac{1}{2}Cr_3C_2 : (+) \\ 3F^- + \frac{1}{2}Cr_3C_2 = 3e + \frac{3}{2}CrF_2 + C_G : (-) \\ \hline C_{CNT} = C_G \end{gathered} \qquad \text{(B)}$$

The main advantage of this kind of cell is that no supplementary thermodynamic data are necessary to derive the thermodynamics of the cell reaction. Only the E vs T experimental data are necessary to obtain $\Delta_r G$, $\Delta_r H$, and $\Delta_r S$ as reported in any chemical thermodynamics textbook.

2.2. Cell Assembly. Figure 2 shows the scheme and a picture of the assembled cell. The E measurements[12,27] were carried out in a high-vacuum vertical furnace using an inconel spring-loaded latticework for positioning the holder of the electrochemical cell in the isothermal zone of the furnace. The vertical force applied to the cell is maintained at a preset value by a feedback motion device in such a way as to compensate for size changes due to the temperature variations. In this way the contact pressure at the electrode/electrolyte interface is independent from temperature. Throughout the experiment the average hydrostatic pressure applied to the cell was 0.120 ± 0.003 MPa. The cell holder containing the electrodes, electrolyte, and Mo lead wires is machined from a workable alumina rod (Aremco, Valley Cottage, NY). Two small holes (1 mm dia.) serve as an outlet for the Mo wires and cell outgassing. All the components of the cell were shaped as small cylinders assembled as a sandwich in which the electrolyte is in the middle. The electrolyte is a polished disk of CaF_2 monocrystal (MolTech GmbH, Germany) (111) oriented, 2 mm thick, and 8 mm diameter.

The electrodes were prepared in a glovebox filled with inert and dry atmosphere according to the criterion of establishing the polyphasic coexistence through a close contact among the powder particles. Following the well-established standard procedure, the pure solid phases, as fine powders, have been mixed in acetone and, after evaporation of the solvent, pressed in a stainless steel mold at 0.6 GPa for obtaining cylinders 6 mm diameter × 3 to 5 mm height. Graphite, CrF_2, and Cr_3C_2 were pure powdered chemicals (99%, 1−2 μm; 97%, 80 mesh; 99%, 325 mesh, respectively) from Aldrich. The weight ratio between Cr_3C_2, CrF_2, and graphite or SWCNTs was about 10:5:1. The surfaces of electrodes were gently polished in such a way as to be flat and in perfect contact with the electrolyte surfaces. The total length of the cells was never greater than 12 mm. Molybdenum wires up to the feedthroughs of the furnace flange realized the electrical leads. The temperature was measured by two S-type (Pt/Pt−Rh 10%) thermocouples, which were calibrated against pure Au melting point. Before starting the E measurements, the system was carefully flushed with Ar (O_2 < 1 ppm, H_2O < 1 ppm) and then outgassed by following a standard procedure, which does not allow any temperature increase of the cell if the pressure inside the furnace is greater than 1×10^{-6} mbar. This procedure requires at least 7 days. The total pressure during the experiment is maintained below 1×10^{-7} mbar. A high impedance preamplifier (10^{15} ohm, typical bias current 40 fA) connected to one of the analog input channels of a data logger was used for the E measurements. The total accuracy, Δ_e, in reading the E was less than 100 μV. Furnace temperature and pressure as well as the E values, were read by the data logger connected to a personal computer running on LabView platform. The stability, Δ_T, of the temperature of the furnace at the set temperature was always within 0.5 K. The temperature changes throughout the experiments were performed by programmed ramps with a slope of |2| K/min.

2.3. Measurement Procedure. The length of each isotherm was at least 5 h with data reading every 180 s at the data logger scan rate of 40 channels s^{-1}. Only the last 30 E, T couples of data points in each isotherm were considered as stationary values provided that their standard deviations σ_e and σ_T were respectively $\leq \Delta_e$, Δ_T. If these conditions were not fulfilled, that isotherm was discarded.

3. Results

Four SEGCs equal to cell A were tested, obtaining a behavior very similar to that reported in Figure 3. Each cell was tested through a run composed by some (two to four) thermal cycles, each comprising 62 isotherms, until disappearance of the E vs T hysteresis. Figure 3 shows that three complete cycles were necessary to obtain reproducible data well fit by a ninth degree polynomial curve. Therefore, $E(T)$ in the temperature range from 750 to 1015 K is given by:

$$\begin{aligned} E(T) = {} & -50.023 + 0.1994T - 0.000229T^2 - \\ & (7.7479 \times 10^{-9})T^3 + (1.1551 \times 10^{-10})T^4 + \\ & (6.4845 \times 10^{-16})T^5 + (4.6124 \times 10^{-19})T^6 - \\ & (1.3633 \times 10^{-20})T^7 - (4.9611 \times 10^{-23})T^8 + \\ & (3.4027 \times 10^{-26})T^9 \end{aligned} \qquad (1)$$

with correlation coefficient equal to 0.99897. The fit residuals are plotted in the bottom panel of Figure 3, and their values are confined between −1.4 and 1.3 mV. The value ±1.4 mV will be considered as maximum error.

According to thermodynamics of reversible electrochemical cells at constant T and P, the changes of free energy, ΔG, enthalpy, ΔH, and entropy, ΔS for $C_{CNT} = C_G$ process are given by:

$$\Delta G = -3FE(T) \qquad (2)$$

$$\Delta S = 3F\dot{E}(T) \qquad (3)$$

$$\Delta H = 3F[T\dot{E}(T) - E(T)] \qquad (4)$$

where F is the Faraday constant and $\dot{E}(T)$ is the first derivative of $E(T)$ with respect to T. Figure 4 shows the above quantities as function of T. Since the quotient $a_{C(G)}/a_{C(CNT)}$ of activities not at

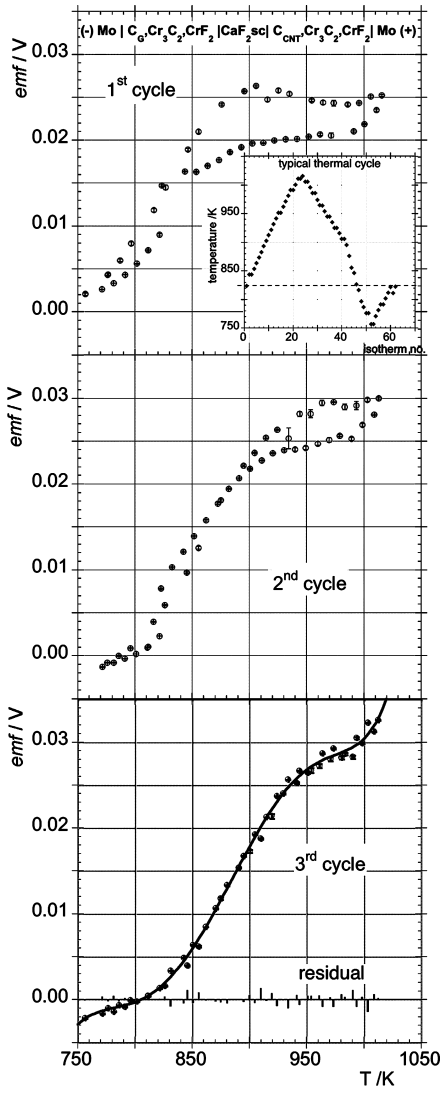

Figure 3. Electromotive force values against temperature of the CaF_2 electrolyte galvanic cell. Three complete thermal cycles were necessary to reach a reproducible behavior. The inset in top panel shows the thermal cycle comprising 62 isotherms, each one lasting at least 5 h. The residuals of the polynomial fit are shown in bottom panel.

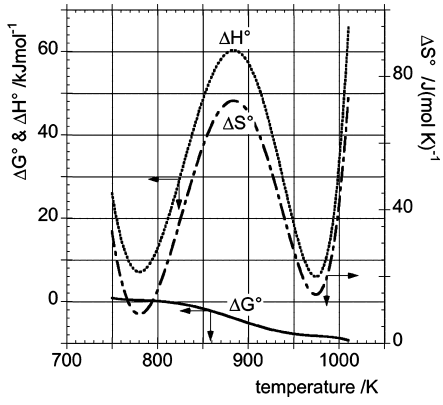

Figure 4. Enthalpy and free energy changes (left axis) and entropy change for the cell transformation from carbon in SWCNT bundles to carbon in graphite calculated according to eq 2−4 from the electromotive force data.

equilibrium is unity, $\Delta G_T = \Delta G^\circ_T$. At 805 K, $E(T) = 0$ (see Figure 3, bottom panel), $\Delta G_{805} = \Delta G^\circ_{805} = 0$ and $\Delta\mu^\circ_C = 0$.

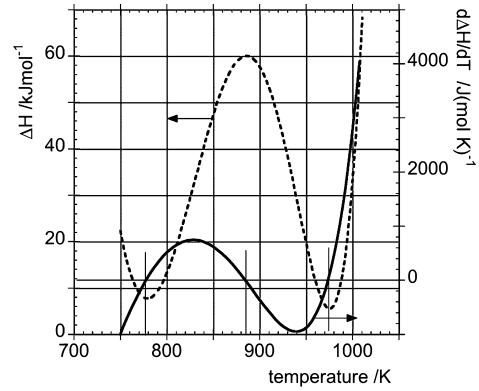

Figure 5. Enthalpy change (left axis) and its first derivative with respect to temperature (right axis).

Table 2. Room Temperature Data for Computing Eq 6[a]

	α, K^{-1}	β, Pa^{-1}	V, $m^3\ mol^{-1}$
Cr_3C_2	1.04×10^{-5} (ref 31)	3.04×10^{-12} (ref 30)	2.70×10^{-5}
SWCNT bundle[b]	4.20×10^{-5} (ref 32)	1.90×10^{-11} (ref 23)	9.02×10^{-6} (ref 22)
graphite	2.60×10^{-5} (ref 32)	2.68×10^{-11} (ref 33)	5.30×10^{-6}

[a] α, β, and V are respectively the molar volume expansion coefficient, the coefficient of compressibility, and molar volume. [b] SWCNT (10,10).

4. Discussion

4.1. Thermodynamic Data. The presence of a vanishing hysteresis in the emf trend demonstrates that the whole system of SWCNTs in the bundles and bundles themselves changes to reach new stable configurations that convert reciprocally and reversibly as function of temperature. This is quantitatively proved by the standard enthalpy and entropy changes, ΔH°_T and ΔS°_T, where both have similar trends in the same temperature interval passing through two minima at 778 and 975 K separated by a maximum at 883 K. At these temperatures ΔH°_T and ΔS°_T are respectively 7.1, 6.0, and 60.2 kJ mol^{-1} and 8.6, 14.7, and 72.8 J K^{-1} mol^{-1}. By further elaboration of enthalpy data of Figure 4, we see in Figure 5 that the values of $d\Delta H/dT$ largely exceed Δc_p, i.e., the molar heat capacity difference between the two carbon forms that is expected close to zero at the explored temperatures. Therefore, the $d\Delta H/dT$ values should be attributed practically only to the behavior of the CNT bundles. If some phase transition occurs, the equilibrium pressure does not remain constant, as the temperature is varied and the equation

$$\frac{d\Delta H}{dT} = \Delta c_p + \left[\Delta V - T\left(\frac{\partial \Delta V}{\partial T}\right)_p\right]\frac{dP}{dT} \approx [\Delta V - T\Delta(\alpha V)]\frac{dP}{dT} \quad (5)$$

should be considered,[29] where α is the molar volume expansion coefficient, $\Delta V = V_G - V_{CNT}$ and $\Delta(\alpha V) = \alpha_G V_G - \alpha_{CNT} V_{CNT}$. V is the molar volume. The pressure, P, is the *internal* pressure to which the graphite and CNTs in the respective highly compacted electrodes of the SEGC are subjected. Cr_3C_2 and graphite or CNTs are respectively the major and minor component present in the electrodes. As reported in Table 2, at room temperature, the coefficient of compressibility, β,[30] and

(29) Klotz, I. M., Rosemberg, R. M. *Chemical Thermodynamics*, 7th ed.; John Wiley & Sons, Inc.: New York, 2008; p 200.

α[31] of Cr_3C_2 are significantly lower than those of CNTs[32,23] and graphite.[32,33] Therefore, as CNTs and graphite are caged into a matrix of Cr_3C_2 particles, such differences are responsible for a real constraint to the thermal expansion of SWCNT bundles, i.e., they can be imagined as being in a multianvil press. Assuming that the electrode volume, V_e, is practically constant with temperature, the equation

$$\left.\frac{dP}{dT}\right|_{Cr_3C_2,C} = -\frac{\left(\frac{\partial \Delta V_e}{\partial T}\right)_P}{\left(\frac{\partial \Delta V_e}{\partial P}\right)_T} = \frac{\alpha_{Cr_3C_2}V_{Cr_3C_2} - \alpha_C V_C}{\beta_{Cr_3C_2}V_{Cr_3C_2} - \beta_C V_C} \quad (6)$$

holds to check the possibility that CNTs were experiencing an increasing internal pressure with temperature. The subscript C stands for graphite or CNTs. By eq 6, the quantity $dP/dT|_{Cr_3C_2,C}$ was found to be 1.1 and -2.4 MPa K^{-1} for CNTs and graphite, respectively. Contrary to the electrode containing graphite, by increasing temperature, CNTs are subjected to high internal pressure changes, which are mostly due to the reversible transformations in the SWCNT bundles. The internal pressure represents how the internal (cohesion) energy, $\Delta\varepsilon$, of the SWCNT bundles, changes by volume, i.e., $(\partial\Delta\varepsilon/\partial V)_T$.

Equation 5 can be now utilized to obtain the cohesion energy by writing that:

$$\left(\frac{\partial \Delta\varepsilon}{\partial V}\right)_T = \Delta P \approx \int_{Tr}^{T} \frac{d\Delta H}{dT} f^{-1}(T)dT \quad (7)$$

where

$$\begin{aligned} f(T) &= V_{G,Tr}(1 - \alpha_G T)e^{\alpha_G(T-Tr)} - \\ &\quad V_{CNT,Tr}(1 - \alpha_{CNT}T)e^{\alpha_{CNT}(T-Tr)} \\ &\approx V_{G,Tr} - V_{CNT,Tr} = -3.64 \times 10^{-6}\ m^3\ mol^{-1} \end{aligned} \quad (8)$$

Tr being the room temperature and $V_{i,Tr}$ the molar volume at Tr. By numerical integration of eq 7 and taking into account the average molar volume[22] of SWCNT bundles, the energy change, $\Delta\varepsilon$, was found and plotted against temperature in Figure 6. Three different energy states, C_{b0}, C_{b1}, and C_{b2} of carbon in different bundle configurations can be identified in Figure 6 at 778 and 975 K where the minima are located and at maximum at 883 K. The C_{br} state in the same figure corresponds to the van der Waals equilibrium energy calculated[23] as temperature independent for a bundle of tubes of a given type (n,m). Armchair tubes $n = m$ (10,10) are considered in Figure 6. Some values of deviations $(L-L_{eq})$ from the equilibrium distance $L_{eq}(r) = 1.6723$ nm are reported as a function of energy according to temperature independent calculations indicated in literature.[23] Here, such calculated values were considered at Tr = 298 K.

Each $\Delta\varepsilon_x$ value represents the energy change of transformation C_{bx} (Tx) $\rightarrow$ C_{br} (Tr) given by $\Delta\varepsilon_x = \int_{Tx}^{Tr} c_v(C_{bx})dT + u_x(Tr)$ where c_v and u_x are respectively the molar heat capacity at constant volume and transformation energy of C_{bx} at Tr.

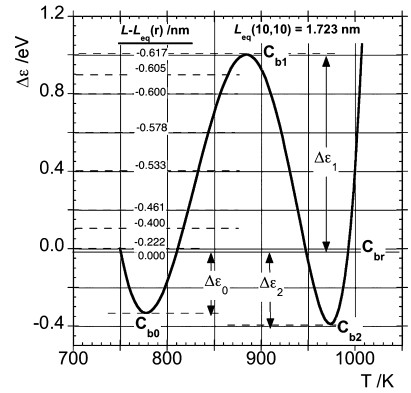

Figure 6. Cohesion energy, $\Delta\varepsilon$, of SWCNTs in the bundles as a function of temperature calculated by eq 7 through eq 8. Different states, C_{bx}, of tubes in the bundles are identified at minima and at maximum. The state C_{br} is the equilibrium state of (10,10) armchair tubes in a perfect triangular closed packed arrangement with L_{eq} lattice constant. Some $L-L_{eq}$ distances matching the cohesion energy calculated[23] through the continuum model are displayed.

It is important to remind that all thermodynamic quantities plotted in Figure 4 refer to transformations $C_{bx} \rightarrow C_G$ at $T =$ Tx, which is in fact the cell reaction. Therefore, we are dealing with path $C_{bx} \rightarrow C_{SWCNT} \rightarrow C_G$ at the same temperature where C_{SWCNT} is carbon in unbundled SWCNTs. To determine the thermodynamics of $C_{SWCNT} \rightarrow C_G$, the thermodynamics of $C_{bx} \rightarrow C_{SWCNT}$ should be known. In practice, the entropy of the latter transformation, that is, the entropy change related to the van der Waals assembly of SWCNTs to form a bundle, is unknown. It is however possible to calculate the enthalpy change. For $C_{bx} \rightarrow C_G$, ΔH°_{298} is given by $\Delta H^\circ_{298} = \Delta H^\circ_{Tx} - \int_{298}^{Tx} \Delta c_p dT \approx \Delta H^\circ_{Tx}$ where ΔH°_{Tx} is the experimental value. The approximation is reasonable since expected to be within the maximum experimental error ($\pm 3 \times F \times 1.4 \times 10^{-3} = \pm 0.4$ kJ mol^{-1}) because of $\Delta c_p \approx 0$. From Lennard–Jones type calculations[21–23] of potential of SWCNTs in a bundle, the energy associated to transformation $C_{bx} \rightarrow C_{SWCNT}$ is available. Therefore, by combining the sequence of transformations as

$$\begin{aligned} C_{b0} &\xrightarrow{\Delta_0 H^\circ_{298}} C_{SWCNT} \\ C_{b1} &\xrightarrow{\Delta_1 H^\circ_{298}} C_{b0} \\ C_{b2} &\xrightarrow{\Delta_2 H^\circ_{298}} C_{b1} \\ C_G &\xrightarrow{\Delta_G H^\circ_{298}} C_{b2} \\ \hline C_G &\xrightarrow{\Delta_S H^\circ_{298}} C_{SWCNT} \end{aligned} \quad (9)$$

where $\Delta_1 H^\circ_{298}$, $\Delta_2 H^\circ_{298}$, and $\Delta_G H^\circ_{298}$ are experimentally determined (see Figure 4) and equal to -52.2, 54.4, and 5.6 kJ mol^{-1}, respectively. $\Delta_0 H^\circ_{298}$ is 1.96, 1.69, and 1.55 for SWCNT bundles with (8,8), (10,10), and (12,12) SWCNTs.[23] Because the differences between those values are within the maximum experimental error, we can assume 1.7 kJ mol^{-1} as the averaged value. Therefore, $\Delta_S H^\circ_{298} = 9.5 \pm 0.4$ kJ mol^{-1} (98 $\pm$ 4 meV). This result is 15% higher than the $\Delta_f H^\circ_{298}$ of MWCNTs previously found[12] by making use of the same technique.

(30) Jiang, C. *Appl. Phys. Lett.* **2008**, *92*, 041909.
(31) Scabarozi, T. H.; Amini, S.; Leaffer, O.; Ganguly, A.; Gupta, S.; Tambussi, W.; Clipper, S.; Spanier, J. E.; Barsoum, M. W.; Hettinger, J. D.; Lofland, S. E. *J. Appl. Phys.* **2009**, *105*, 013543.
(32) Maniwa, Y.; Fujiwara, R.; Kira, H.; Tou, H.; Kataura, H.; Suzuki, S.; Achiba, Y.; Nishibori, E.; Tarata, M.; Sakata, M.; Fujiwara, A.; Suematsu, H. *Phys. Rev. B* **2001**, *64*, 241402.
(33) Blakslee, O. L.; Proctor, D. G.; Seldin, E. J.; Spence, G. B.; Weng, T. *J. Appl. Phys.* **1970**, *41*, 3373.

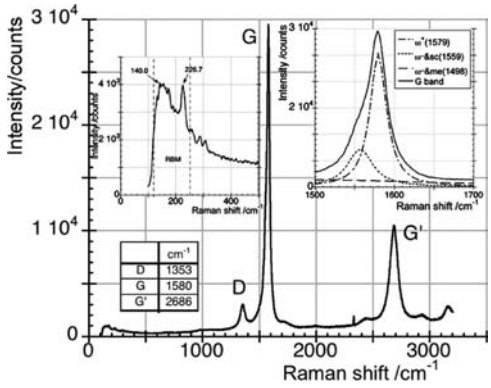

Figure 7. MicroRaman spectra at Ar+ laser excitation ($\lambda = 514.5$ nm) of the as-received sample. The left side inset displays the spectrum portion related to the radial breathing mode (RBM) where information on the tube diameter can be obtained through eq 10. The right side inset shows that two features constitute the G band.

No experimental data are reported in literature to compare the above results. Just one theoretical work[11] concerning the transformation $C_G \rightarrow C_{bx}$ can be utilized to make some comparisons. From the dependence of formation energy by tube radius, r_t, bundle radius, r_b, and ratio, M_{57}, between the pentagons and heptagons on hexagons, the value of $\Delta_G H^\circ_{298} = 5.6$ kJ mol^{-1} ($C_G \rightarrow C_{b2}$) matches with $r_t = 0.695$ nm at $M_{57} = 6.45 \times 10^{-4}$, $r_b = 17$ nm at $M_{57} = 6.48 \times 10^{-4}$ and $r_t = 0.6958$ nm, and $M_{57} = 5.75 \times {}^{-4}$ at $r_t = 0.6958$ nm. The entropy was estimated, at $r_b = 17$ nm and $\Delta_G H^\circ_{298} = 5.6$ kJ mol^{-1}, to be 65 J K^{-1}mol^{-1} from the plot of the free energy change vs r_b calculated at $M_{57} = 6.485 \times 10^{-4}$ and $r_t = 0.6958$ nm. The value should be compared with the present value of 14.4 J K^{-1}mol^{-1} for C_{b2} at 975 K. The corresponding free energy change calculated at 1500 K is about -93 kJ mol^{-1} to compare with -8.4 kJ mol^{-1} at 975 K. It is worth noticing that in the above theoretical calculation, enthalpy and entropy are considered temperature independent while the free energy change was computed at 1500 K. Because of this and the necessary simplifications of the theoretical approach the comparison is not completely satisfactory. Notwithstanding such discrepancies, the average tube and bundle diameters should be respectively close to 1.4 and 34 nm. These values are well in agreement with our observations (see further on). Supposing a perfect tightly packed triangular bundle with lattice parameter $L = 2r_t + b$ with $b = 0.34$ nm as the least distance between two adjacent nanotubes, bundles with 360 equal diameter tubes should be expected.

To shed light on this behavior, it is necessary to investigate the status of SWCNT bundles before and after the experiments, making some assumptions on the phenomena that occurred in situ meanwhile in the experiment. It is worth noticing that all the features below will refer to a sample cooled to room temperature.

4.2. Structural Data. Figures 7 shows the mR spectrum of the as-received SWCNTs, which is comparable with the spectrum given by the supplier. In the left side inset is reported the spectrum section characteristic of the radial breathing mode[34] (RBM) of SWCNTs. According to literature,[35] the Raman features appearing between 120 cm^{-1} < ω_{RBM} < 250 cm^{-1} correspond to the atomic vibration of the C atoms in the radial direction, as if the tube was breathing. These features depend of the nanotube diameter, d_t, through relation

$$\omega_{RBM} = A/d_t + B \qquad (10)$$

where A and B are experimentally determined to be respectively 234 and 10 cm^{-1} for typical SWCNT bundles with 1 nm < d_t < 2 nm. Outside this interval, eq 10 does not hold because for d_t < 1 nm there is a chirality dependence of ω_{RBM} and for d_t > 2 nm the features are very weak. Therefore, a bimodal distribution of diameters at 1.08 and 1.80 nm could be present in our sample. Looking at the right side inset of Figure 7, where the G band is magnified, we can observe that the feature is not perfectly symmetric due to the superimposition of other features well separated by two Lorentzian lineshapes named G^+ and G^- that are generally the most intense ones. Semiconducting and metallic SWCNTs can be differentiated through the G^- feature, which is broadened for metallic SWCNTs. At a given d_t, ω_{G-}(semiconducting) > ω_{G-}(metallic) whereas $\omega_{G+} > \omega_{G-}$ and ω_{G+} is practically d_t independent. In the case of bundles, no precise information can be derived on the SWCNT semiconducting nature because of the diameter distribution. In the present case, the G^- position and its broadening as well as the diameter range indicate metallic type SWCNTs. The quantity $\Delta\omega = \omega_{G+} - \omega_{G-}$ can be roughly related to the maximum in the Gaussian diameter distribution of the sample.[36] Figure 8 shows the mR spectra of SWCNTs in the SEGC electrode after the experiment

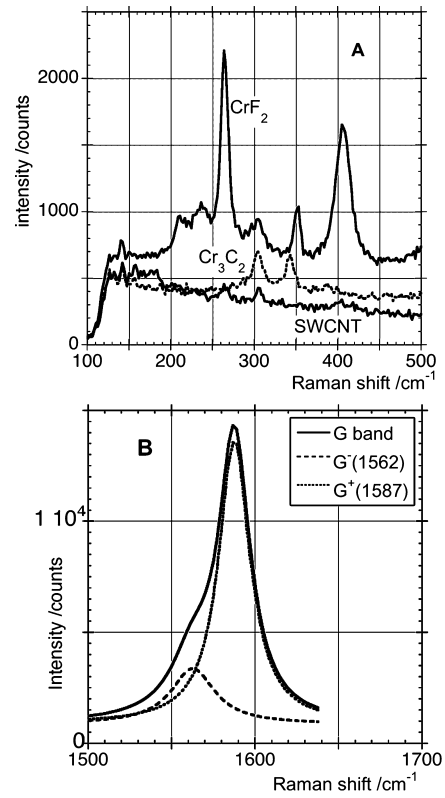

Figure 8. microRaman spectra at Ar+ laser excitation ($\lambda = 514.5$ nm) of the SEGC electrode containing SWCNT bundles after the experiment. Panel A shows the presence of all the components of the electrode. The characteristic features of RBM of SWCNTs disappeared. Panel B shows that the G band of SWCNTs is practically unchanged with respect to the initial sample.

(34) Jorio, A.; Pimenta, M. A.; Souza Filho, A. G.; Saito, R.; Dresselhaus, G.; Dresselhaus, M. S. *New J. Phys* **2003**, *5*, 139.
(35) Milnera, M.; Kürti, J.; Hulman, M.; Kuzmany, H. *Phys. Rev. Lett.* **2000**, *84*, 1324.
(36) Kasuya, A.; Sasaki, Y.; Saito, I.; Tohji, K.; Nishina, Y. *Phys. Rev. Lett.* **1997**, *78*, 4434.

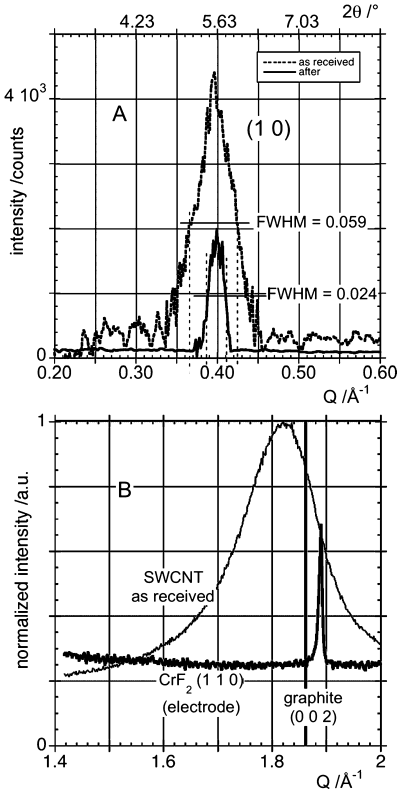

Figure 9. XRD spectra at Cu Kα radiation. Panel A shows the low angle spectra of as-received (dashed line) and heat-treated SWCNT bundles. Panel B shows the portion of the spectrum around the (0 0 2) graphite feature. The peak of SWCNTs in the electrode after the experiment is not detected because of the low mass inside.

and in the as-received sample. The spectra of Cr_3C_2 and CrF_2 are compared in panel A with the spectrum of the SEGC electrode in the RBM region. The features of RBM disappeared. This is attributed to the superimposition of the features of the other components that make the weak RBM band practically undetectable. The line shape of the G bands is practically the same though there is a 9 cm^{-1} upshift with respect to the initial sample. This similar shift behavior of the G^- feature means in the case of isolated SWCNTs a diameter increase, as found in the literature.[37]

The low angle XRD analysis is reported in Figure 9A. The comparison of XRD spectra, both with background subtracted, between the as-received SWCNT sample and a SWCNT sample, which was thermally cycled as the SWCNTs in the SEGC electrode (the SWCNT quantity in the SEGC electrode is too low to be detected by XRD), is reported. Abscissas are labeled in 2θ and $Q = 4\pi/\lambda \sin\theta$, the scattering vector, where Cu Kα radiation (λ = 0.154184 nm) was used. In the Q region 0.30−0.50 $Å^{-1}$, both peaks are positioned close to 0.4 $Å^{-1}$, but the line shapes are different.

It is was found[38] that:

• The fwhm, ΔQ, of the (10) Bragg peak only depends on the diameter of the bundle, independently of the tube diameter inside. However, ΔQ increases as the diameter dispersion increases.

• The position of the peak depends on the mean tube diameter, diameter of bundles, and tube diameter dispersion.

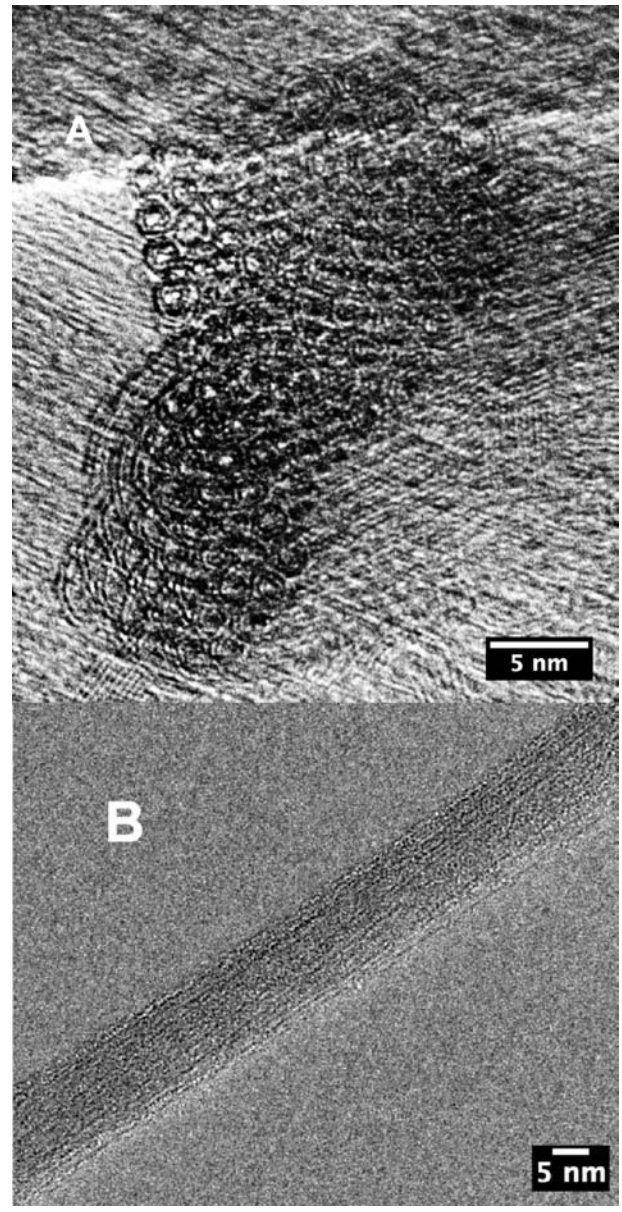

Figure 10. HR-TEM of the as-received sample. Panel A displays the cross section of a bundle with almost regular triangular packing with a lattice constant typical of (10,10) armchair tubes. In panel B, a straight portion of a bundle is shown.

• The intensity is dominated by contribution from the largest tubes.

The peaks in Figure 9A show clearly that changes occurred in the sample. The decrease of ΔQ implies that the average bundle diameter changed from about 20 to 50 nm without any significant change of the average tube diameter, which is 1.4−1.5 nm according to the Q value of the peak. The decrease of the peak intensity could be the result of separation of SWCNTs (mainly those in the outermost position) from its own bundle and their successive aggregation with other smaller bundles. The expected final result of this process could be the formation of large bundles with the largest diameter tubes and bundles unsuitable to contribute to the X-ray diffraction because they are too small. Figure 9B shows in the Q range of the (002)

(37) Jorio, A.; Pimenta, M. A.; Souza Filho, A. G.; Samsonidze, G. G.; Swan, A. K.; Ünlü, M. S.; Goldberg, B. B.; Saito, R.; Dresselhaus, G.; Dresselhaus, M. S. *Phys. Rev. Lett.* **2003**, *90*, 107403.

(38) Rols, S.; Almairac, R.; Henrard, L.; Anglaret, E.; Sauvajol, J.-L. *Eur. Phys. J. B* **1999**, *10*, 263.

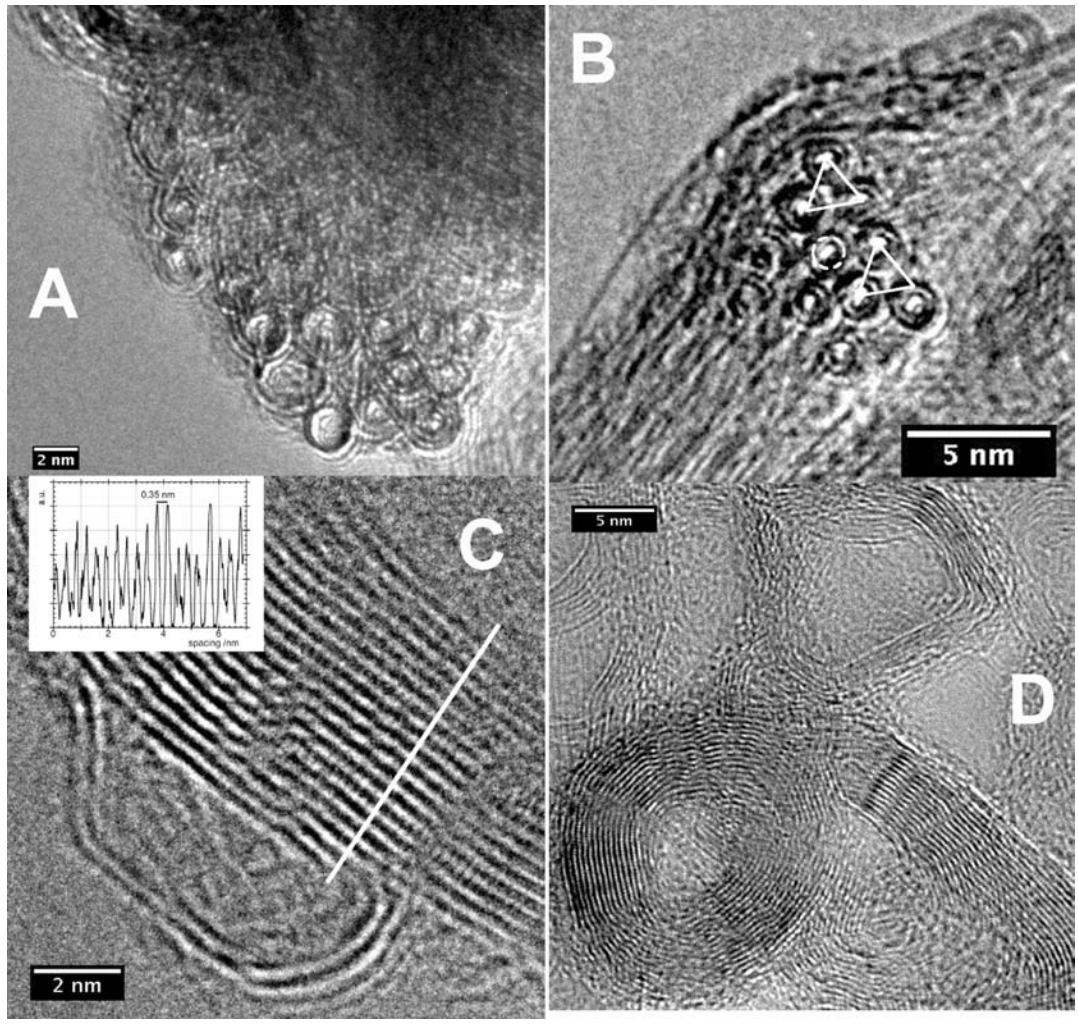

Figure 11. HR-TEM of SWCNT bundles in the SEGC electrode after the experiment. Panels A and B show the cross sections of two SWCNT bundles that are differently deformed: ellipsoidal modifications of large tubes (A) and lattice irregularities (B, white triangles superimposed) but tubes with almost regular shape (white dashed circle). Panel C shows the separation of a tube from a bundle. The inset gives the profile along the white line. Different type interfringe irregularities are present on both sides of the white line. The apparent fusion of bundles is shown in panel D.

peak of graphite[39] the features of the as-received sample and the SEGC electrode, where no graphite-like feature appears because of low SWCNT mass content. The SWCNT sample thermally treated as previously did not show any appreciable difference with respect to the as-received sample. In both cases, the peak position gives $d_{002} = 0.3453$ nm to compare with 0.3376 nm of graphite.

SWCNTs in the as-received sample and in the SEGC electrode were extensively analyzed by HR-TEM to look for morphological changes compatible with high temperature transitions which were observed through the thermodynamic quantities associated to transformation $C_{CNT} = C_G$. Figure 10 shows the bundle nature of the sample by the cross section (panel A) and longitudinal (panel B) views. These images are very similar to those reported in literature.[40] The internal organization of the tubes in the bundle appears to be almost regular according to a close-packed triangular arrangement. The two-dimensional lattice constant, L, was estimated to be close to 1.7 nm, which is compatible with the armchair (10,10) tube diameter (1.357 nm) and intertube distance, $b = 0.345$ nm, as found by the (002) XRD feature. The four panels of Figure 11 display the HR-TEM analysis performed on the SWCNTs in the SEGC electrode after the experiment. The cross sections of two bundles are reported in panels A and B. In both images, tubes and/or closed-packed arrangement show strong deformations that were not found in the original sample. The superimposed triangles in panel B demonstrate a distorted lattice though the tube cross section appears to be almost regular (see the superimposed white dashed circle). Panels C and D display the side view of bundles where the heat treatment produced deep changes such as to separate tubes (panel C) or to "fuse" bundles together (panel D). The line profile along the white line in the inset of panel C shows a constant spacing corresponding to 0.35 nm. It is clearly visible that just on the left and right sides of that line the regularity of the interfringe distance is seriously damaged.

In order to merge all the above information into a coherent scenario with the thermodynamic data, we have to assume that each equilibrium point in the bottom panel of Figure 3, at a given T and internal pressure P, represents a deformation of the two-dimensional lattice that involves both the lattice parameter, L, and tube shape. Theoretically, the cohesion energy among tubes in a bundle has been extensively studied by the

(39) JCPDS-International Center for Diffraction Data, 2001 data base card = 41−1487.
(40) Colomer, J.-F.; Henrard, L.; Lambin, P.; Van Tendeloo, G. *Eur. Phys. J. B* **2002**, *27*, 111.

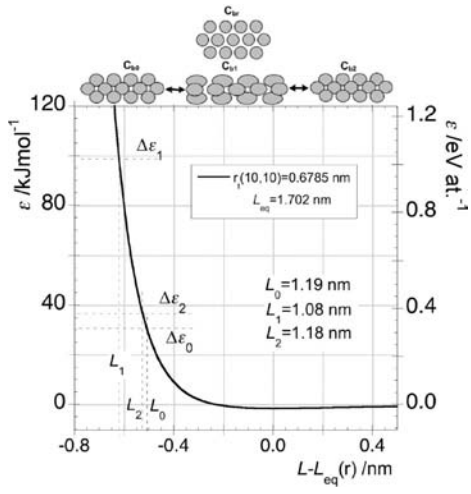

Figure 12. Cohesive energy of a bundle of (10,10) armchair tubes calculated[23] by the continuum model. The distances L_i calculated at $\Delta\varepsilon_i$ (Figure 6) are reported. The schematic drawing represents qualitatively the bundle states supposed existing as function of temperature.

continuum model.[21,23] This is customary for solids where the cohesion depends on the van der Waals interactions and Lennard−Jones, LJ, potential holds. The equation below[23] gives the dependency of ε from the distance L between the centers of two adjoining tubes as:

$$\varepsilon(L) = -\frac{|\varepsilon(L_{eq})|}{0.6}\left[\left(\frac{L_{eq}}{L}\right)^4 - 0.4\left(\frac{L_{eq}}{L}\right)^{10}\right] \qquad (11)$$

where

$$|\varepsilon(L_{eq})| = \frac{A_a}{2\pi r}(-0.1135r^{1/2} + 9.39 \times 10^{-3}) \qquad (12)$$

The term in parentheses gives the equilibrium potential[23] in eV/Å as a function of the tube radius, r, while the term outside needs to convert to eV/at. C. A_a is the area of a carbon atom (2.62 Å^2). Figure 12 shows the curve ε vs $L - L_{eq}$ calculated according to eq 11 for a bundle of (10,10) armchair tubes. The L_i distances corresponding to the $\Delta\varepsilon_i$ values reported in Figure 6 are also displayed. The distances corresponding to the bundle arrangements C_{b0}, C_{b1}, and C_{b2} are, respectively, 1.19, 1.08, and 1.18 nm. All these values are lower than $2r = 1.3657$ nm, which is the minimum nonequilibrium distance between two (10,10) tubes. To shorten this distance to the L_i values, it is necessary to introduce the tube deformation as already found in high pressure experiments but at room temperature.[17−20,24] One of these works[17] assumes that the tube deformation occurs through flattening along the diameter instead of through the polygonization of the tube circumference. Obviously, the LJ calculations do not consider the contribution of energy deformation, which can be estimated[21] equal to be $A_a(\rho^{-1} - r^{-1})c_0/2r$ where, $c_0 =$ 1.02 eV is the elastic energy for bending the graphene sheet and ρ is the curvature radius produced by the deformation. The scheme in Figure 12 gives just an idea how the arrangements C_{bx} should be imagined. Considering the L_i values, the tubes in C_{b0} and C_{b2} are moderately deformed, almost ellipsoidal, the minor axis being reduced by 13.0 and 13.7% with respect to the tube radius, respectively. Because of high internal pressure and temperature, a further deformation allows the slipping of planes in the triangular packing, producing the arrangement C_{b1} where the interaction becomes highest. The arrangement C_{b2} is formed when the triangular packing is restored though it is still deformed.

5. Conclusion

In summary, the main results obtained in this work are as follows:

• The experimental data at high temperatures on the thermodynamics of transformation from graphite to SWCNT bundles were measured in the temperature interval 750−1015 K. No such data can be found in literature.

• The formation enthalpy $\Delta_f H^\circ_{298}$ of unbundled SWCNTs was determined, and this value is consistent with the experimental $\Delta_f H^\circ_{298}$ of MWCNTs found elsewhere[12] by making use of the same kind of SEGCs.

• Because of the combined action of high temperature and constraint on the dilatation of SWCNTs in the bundles, strong modifications of the triangular closed packed lattice of tubes occur. This behavior indicates that three different states were observed in the explored temperature range. Each converts reversibly with the other state as temperature changes.

• The enthalpy, entropy, and free energy changes of these states were determined with respect to graphite.

• The microRaman, XRD, and HR-TEM ex situ analyses confirm that changes really occurred with respect to the initial sample.

• The whole picture is in agreement with high pressure experiments at room temperature in which the polygonization of SWCNTs in the bundle was proposed to justify the observed volume changes.

Acknowledgment. The authors are very grateful to Dr. P.L. Cignini of ISMN-CNR (Roma1 section) for his precious and invaluable technical assistance. The authors (D.G. and A.L.) dedicate this work to Prof. Giovanni De Maria who was a pioneer in Italy of high temperature chemical thermodynamics, distinguished professor of many students, among them the authors, and tireless bearer of new ideas in his long academic career. They are very grateful to him for the present and past illuminating discussions on the widespread implications of the foundations of thermodynamics still that enrich and qualify the teaching of the chemical thermodynamics at SAPIENZA University of Rome.

JA904294Z